Received: 15 July 2022 | Revised: 25 April 2023 | Accepted: 2 May 2023

DOI: 10.1002/jbm.b.35267

RESEARCH ARTICLE

Society For Biomaterials | WILEY

Electrophoretic deposition of gentamicin and chitosan into titanium nanotubes to target periprosthetic joint infection

Greta Della Fara[1] | Adrienn Markovics[1] | Simona Radice[1] | John L. Hamilton[1] | Roberto Chiesa[2] | Andreas Sturm[3] | Katja Angenendt[3] | Alfons Fischer[1,3] | Markus A. Wimmer[1]

[1]Department of Orthopedic Surgery, Rush University Medical Center, Chicago, Illinois, USA

[2]Department of Chemistry, Materials and Chemical Engineering "Giulio Natta", Milan, Italy

[3]Max-Planck-Institut für Eisenforschung GmbH, Düsseldorf, Germany

Correspondence
Adrienn Markovics, Rush University Medical Center, 1735 W Harrison St, Chicago, IL 60612, USA.
Email: adrienn_markovics@rush.edu

Abstract

Periprosthetic joint infection (PJI) occurs in 1%–2% of primary total hip and knee arthroplasties; the rate can reach 20% in individuals at risk. Due to the low local bioavailability of systemic antibiotics and possible off-target effects, localized drug delivery systems are of great importance. Our aim was the electrophoretic deposition (EPD) of gentamicin and chitosan in Titanium (Ti) nanotubes to establish a local, prolonged antibiotic delivery. Nanotubes were created on Ti wire with a two-step anodization process. For drug deposition, EPD and the air-dry methods were compared. For a prolonged drug release, gentamicin and crosslinked chitosan were deposited in a two-step EPD process. Drug release was quantified by fractional volume sampling. The Ti wires were tested against *Staphylococcus aureus* by agar dilution and liquid culture methods. MC3T3-E1 osteoblastic cell viability was determined with trypan blue. Nanotubes were characterized by a 100 nm diameter and 7 μm length. EPD allowed a higher amount of gentamicin deposited than the air-dry method. Drug deposition was controllable by adjusting the voltage and duration of the EPD process. The crosslinked chitosan layer allowed diffusion-driven release kinetics for up to 3 days. Gentamicin-loaded Ti wires significantly inhibited bacterial growth and resulted in a larger inhibition zone compared to unloaded wires. Twenty-four hours of incubation with loaded wires did not have a significant effect on osteoblast viability. Gentamicin-loaded Ti nanotubes represent a promising approach for PJI prevention, as well as a valuable preclinical tool for the investigation of localized drug delivery systems created on Ti surface.

KEYWORDS
electrophoretic deposition, infection, nanotube, periprosthetic, titanium

1 | INTRODUCTION

Primary hip and knee arthroplasty ranks among the top 5 most common procedures performed each year across all surgical disciplines in the United States.[1] Among post-operative complications, periprosthetic joint infection (PJI) is the most common reason for revision and re-revision of implants.[2] Almost 1%–2% of patients undergoing knee or hip replacement develop PJI, and this rate can be over 20% in patients with risk factors.[3] *Staphylococcus aureus* (*S. aureus*) accounts for 20%–30% of cases of orthopedic device-related infections.[4–7]

Different strategies have been implemented to prevent infection at the surgical site[8]; nevertheless, the development of PJI remains a significant problem.[9] Nowadays, PJI prevention and

treatment strategies include prolonged systemic antibiotic administration, which has limitations such as low efficiency, poor bioavailability and distribution, lack of selectivity, potential drug overdose and toxicity in non-target tissues[10] as well as the spread of antibiotic resistance.[11] To overcome this issue, localized drug delivery systems like the incorporation of antibiotic in the bone cement,[12] beads and dissolvable sponges are commonly used.[13,14] Gentamicin is an aminoglycoside antibiotic, exerting a concentration-dependent bactericidal effect against the majority of microbes associated with PJI.

Titanium (Ti) and its alloys are recognized as joint replacement materials due to their excellent biocompatibility, moderate elasticity, and high corrosion resistance.[15] In addition, Ti can spontaneously form a stable and inert layer of titanium oxide (TiO_2) on its surface making it one of the most widely used materials for metallic implants.[16] When the oxide layer is manipulated at the nanoscale, arrays of nanopores, nanopillars or nanotubes can be created.[17] Nanotubes are cylindrical hollow structures with diameters ranging from 1 to 800 nm and they provide an improved level of osseointegration, anti-inflammatory/antimicrobial function and shielding/scaffolding effects.[18,19] Ti surface coatings containing antibiotics have been investigated in recent years.[20–24]

Several animal models have been developed to study PJI.[25,26] Our group and others have successfully investigated PJI previously in a mouse PJI model; to mimic the implant, an orthopedic-grade stainless steel Kirschner wire was inserted in the knee joint of the mouse.[27,28]

The aim of the present study was to create a nanotubular structure on Ti alloy Kirschner wire and to establish a localized, prolonged antibiotic delivery through EPD of gentamicin and chitosan.

2 | MATERIALS AND METHODS

Titanium alloy (Ti6Al4V) ELI wires (0.6 mm diameter, 30 mm length) were purchased from Custom Wire Technologies (Port Washington, WI). The following items were purchased from the indicated sources: gentamicin sulfate, chitosan, sodium tripolyphosphate, ammonium fluoride, ethylene glycol, absolute ethanol, ninhydrin-Millipore Sigma (St. Louis, MO); methanol-Fisher Scientific (Waltham, MA); *S. aureus* Xen36-Perkin Elmer (Waltham, MA), acetone-VWR Chemicals (Radnor, PA).

2.1 | Nanotube creation and characterization on Ti wire

Titanium ELI wires were sonicated in acetone and in methanol for 10 min each to remove any contamination. Nanotubes were fabricated on the wire by anodization.[29,30] First, an ethylene glycol-based solution with 0.3 wt% of ammonium-fluoride (NH_4F) was prepared 24 h prior use to ensure complete NH_4F dissolution. The anodization setup is illustrated in Figure 1A. Briefly, the Ti wire (anode) was positioned in the middle of a hollow graphite cylinder (cathode). A power supply (Delta Elektronika BV SM700) was used to provide the required voltage and the process was performed under a chemical fume hood. Different anodization voltages and times were tested for their effect on nanotube diameter and length. Furthermore, a two-step anodization process (1 h anodization at 70 V followed by 15 min of sonication in methanol, and an additional 30 min of anodization at 70 V) was tested as described to be an effective method to create highly ordered nanotubes.[31,32]

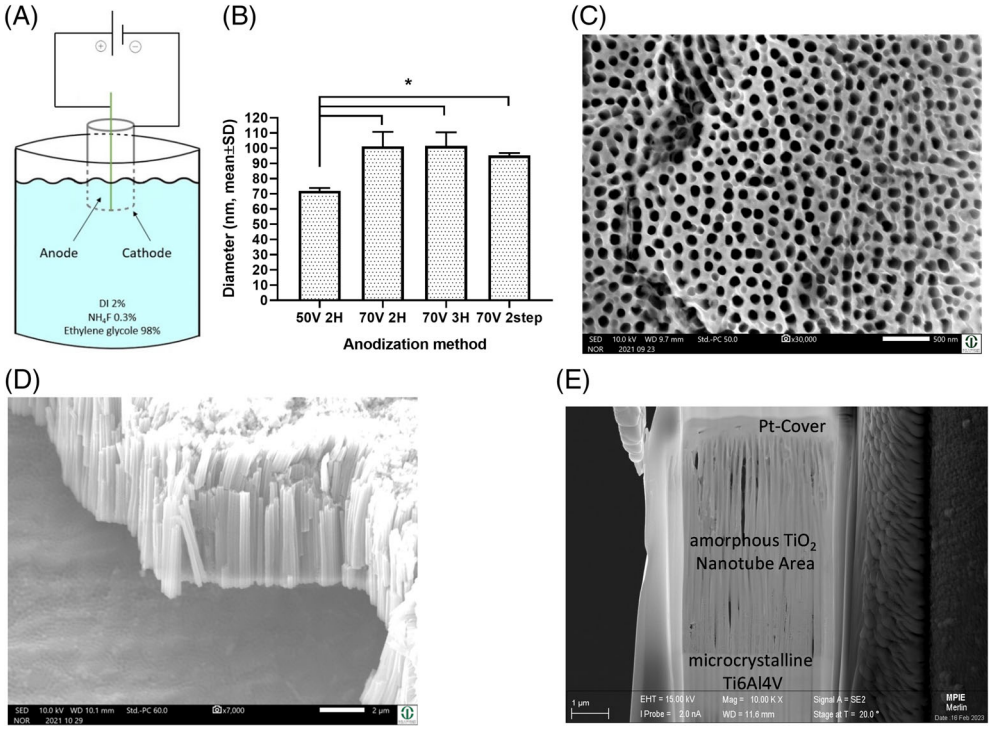

FIGURE 1 Titanium anodization process and nanotube morphology. (A) Schematic illustration of the anodization setup (B) Higher anodization voltage resulted in a significantly larger nanotube diameter ($n = 2–7$/group, $^*p < .05$, one-way ANOVA). (C) SEM top view of 100 nm nanotubes created by anodization (30,000x). (D) Side view of the fractured nanotubular film to estimate thickness (7000x). (E) FIB cut as seen by SEM (10,000x). Note that the nanotubular structure reaches from the Ti6Al4V substrate to the PT-cover. (The structure within the substrate is an artifact generated during FIB polishing within the substrate to gain a thickness of about 30 nm within the tubular area).

The morphology of nanotubes was first assessed using a Scanning Electron Microscope (SEM, Jeol JSM-IT500HR inTouchScope). A 10 kV acceleration voltage and a working distance of 9.8 mm were used to view the surface of the anodized coating and its cross-section after fracturing. In addition, for a more detailed analysis, focused ion beam (FIB) cross-sections were obtained. Using FEI Helios Nanolab 600I and Ga-ions a lamella with a transmittable area of $3.5 \times 7.6\ \mu m^2$ and about 30 nm thickness was cut from the previously characterized SEM section. For protection, a 3 µm thick Pt cover was applied and a copper grid was used as carrier. The FIB cuts were then transferred into an SEM (Zeiss Gemini Merlin) for energy-dispersive X-ray spectroscopy (EDS) and electron backscatter diffraction (EBSD) analyses.

2.2 | Drug loading and coating

Gentamicin sulfate was used as an antimicrobial drug and loaded by EPD. The loading solution consisted of 30% 50 mg/mL gentamicin in distilled water (DI) and 70% of absolute ethanol. All EPD solutions contained ethanol to prevent water hydrolysis. The EPD setup is illustrated in Figure 2B. In the electrochemical cell, the anodized titanium wire represented the cathode, and the platinum wire represented the anode. The latter was arranged as a spiral around the cathode in order to obtain a uniform deposition in all directions. A potential difference of varying magnitude (−4 V and −10 V) was applied using an Interface 1010E potentiostat (Gamry Instruments) with a two-electrode set-up. The setup was placed on a magnetic stirrer to ensure thorough mixing. To determine the efficiency of the EPD method, the air dry method (ADM) was compared to EPD performed at different voltage and time. For both methods, 100 mg/mL gentamicin solution was used. As for ADM, 40 µL of gentamicin solution was pipetted over the wire and dried in a desiccator. EPD was performed with different parameters (−4 V, −10 V, 10 and 15 min), and samples were analyzed after 10 min in PBS solution to determine drug deposition. The difference in the weight of the wires before and after loading was compared to the amount of drug loaded based on in vitro release and UV–vis spectroscopy.

Chitosan is a naturally occurring, linear polysaccharide used in biomedical applications due to its biodegradability, non-toxicity and versatility.[33–37] Due to the positively charged nature of chitosan in solutions below pH = 6, EPD can be used to apply a chitosan coating over the nanotube surface. Low-molecular weight chitosan with sodium tripolyphosphate (TPP) crosslinking[38] was used in order to establish an extended drug release. TPP was dissolved in DI at 1 mg/mL concentration, then added dropwise into the chitosan mixture. Gentamicin loading and chitosan coating were applied as a two-step EPD process. In the first step, a solution containing 50 mg/mL gentamicin and 2 mg/mL chitosan was used, while in the second step, a 2 mg/mL chitosan solution was applied. The EPD parameters were −5 V and 5 min for each step.

In order to confirm the deposition of gentamicin in the nanotubes, SEM imaging and EDS were performed on the surface of a loaded wire.

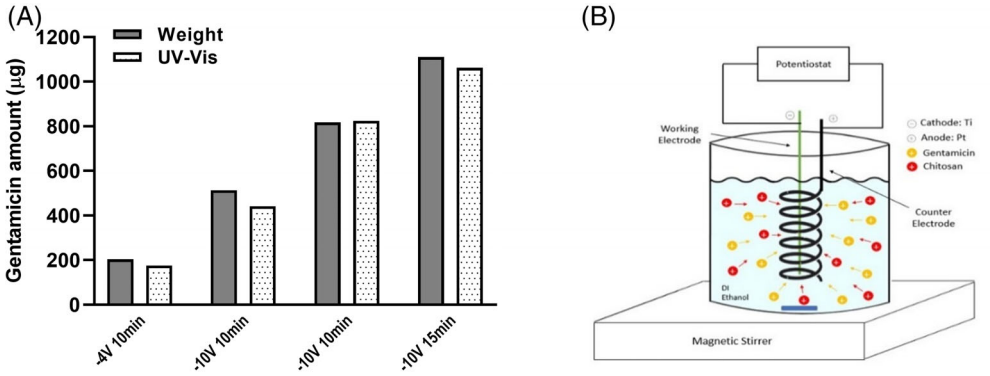

(C)

Weight [µg]	Voltage [V]	Time [min]
84	10	1
333	5	5
363	10	3
440	5	10
513	10	5
667	10	10
870	5	15
1110	10	15

(D)

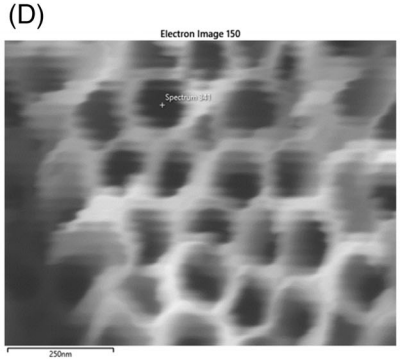

(E)

Spectrum 341	
Element	wt%
C	2.27
O	7.7
F	0.99
Al	2.29
S	2.05
K	0.93
Ti	76.1
V	7.67

FIGURE 2 Electrophoretic deposition of gentamicin and chitosan on anodized Ti wire. (A) Comparison of EPD with different parameters for gentamicin deposition (B) Experimental setup of the two-step EPD (C) Values considered in the multiple linear regression model (D-E) SEM image and EDS assessment of the analyzed point confirms the presence of gentamicin inside the nanotubes.

2.3 | Drug release from the nanotubes

The amount of gentamicin released from the nanotubes was determined by fractional volume sampling. The wire was immersed in 2 mL of PBS (pH = 7.4), constantly stirred and kept at 37°C on a Hot Plate Stirrer (Fisher Scientific, Waltham, MA). 0.2 mL of sample was taken at different time points and replaced with fresh PBS each time. Due to the low absorbance of gentamicin in the visible light range, we used the ninhydrin reaction to determine the optical density.[39] Firstly, gentamicin solutions with known concentrations were prepared in PBS (25, 50, 100, and 500 μg/mL) to establish a standard curve. For the ninhydrin reaction, a 1 w/v % ninhydrin solution was freshly prepared and mixed with the gentamicin solutions at 1:3. The mixture was placed in a 98°C water bath for 15 min followed by cooling on ice for 5 min. The absorbance was determined from the average of 3 readings per sample with a UV–vis spectrophotometer (Nanodrop 2000, Fisher Scientific) at 380 nm. Three different standard curves were established to account for inter-assay variability. Fractional volume sampling of the loaded wires was carried out for up to 3 days. In order to account for the potential interference of chitosan with the ninhydrin assay, wires coated with chitosan only were also tested by fractional volume sampling.

2.4 | Microbiological assessment

To determine the antimicrobial activity of the loaded wires, *S. aureus* (Xen36, derived from ATCC 49525) bacteria were cultured overnight at 37°C in Luria-Bertani medium. The minimal inhibitory concentration (MIC) of gentamicin was determined by the broth dilution method.[40]

In the agar diffusion test,[41] 100 μL of 1×10^6 colony forming units (CFU)/ml *S. aureus* solution was inoculated on agar plates and dried. A gentamicin-loaded chitosan-coated wire, an anodized non-loaded wire and a gentamicin-soaked filter paper were placed on the plate at a distance. The inhibition zone (IZ) around the wires was measured following 24 h incubation at 37°C.

In the liquid broth culture, three tubes with 4 mL of 1×10^5 CFU/ml *S. aureus* were prepared. A gentamicin-loaded chitosan-coated wire was placed in one tube (loaded wire, LW). 0.25 mg gentamicin was added to the second tube (antibiotic control, AC). The third tube contained bacteria only and served as growth control (GC). The tubes were incubated for 24 h, and the absorbance of the solutions was measured with a spectrophotometer (UV-2501, Shimadzu, Japan) in each tube.

2.5 | Osteoblast viability test

Mouse osteoblast-like cell line (MC3T3-E1) was cultured in Dulbecco's Modified Eagle Medium supplemented with 10% fetal bovine serum. Ti wires were placed into the wells of a tissue culture plate. Cells were seeded at 2.5×10^4 cells/cm^2 density and cultured (1) without wire (Cells), (2) with anodized, non-loaded wire (NLW), (3) with gentamicin-loaded wire (LW). Cell viability was determined following 24 h of incubation at 37°C, 5% CO_2, by a Vi-Cell XR cell viability analyzer (Beckman Coulter, Brea, CA).

2.6 | Statistical analysis

Data are presented as mean ± standard deviation. Group means have been tested for statistical significance with one-way ANOVA. Group sizes have been determined based on data obtained with similar methods by others. $p < .05$ was considered statistically significant. Data analysis has been carried out using the GraphPad Prism 9.4.0 statistical software.

3 | RESULTS AND DISCUSSION

3.1 | Nanotube creation on Ti wire

The anodization setup is shown in Figure 1A generated TiO_2 nanotubes on the surface of Ti. We found that higher anodization voltage resulted in a larger diameter, while longer anodization time did not have a significant effect on diameter (Figure 1 B). In samples anodized at high voltage (70 V) or for a long time (3 h), a grass-like structure was obtained, as previously observed by others.[42,43] These samples were sonicated for 5 min in methanol, resulting in the removal of the small collapsed part of the oxide layer. The best morphology was obtained with the two-step anodization method, resulting in larger diameter, open holes, highly ordered nanotubes and low variability in the diameter between samples. Hence, for the subsequent experiments, the two-step anodization process was selected. The nanotubes' surface morphology was investigated by SEM; highly ordered tubular structures showed a 100 nm average diameter at the surface (Figure 1 C). Based on the morphology obtained after fracture of the coating, the nanotubes were estimated to be between 6 and 7 μm in length (Figure 1 D). With a diameter of 0.6 mm of the Ti wire and an 11 mm anodized length, a surface area of about 1700 mm^2 was obtained, compared to 20 mm^2 of the non-treated Ti wire.

The FIB cut revealed an amorphous TiO_2 coating, approximately 5.9 μm in thickness. As shown in Figure 1 E, the titania nanotubes reach from the Ti6Al4V substrate to the Pt-cover. They are not perfectly straight. The black appearances in the image are cut-outs during ion beam polishing at locations where the tube walls became too thin. EDS areal distribution of O and Ti showed a strong and clean demarcation line, separating substrate from coating (shown in supplement). Based on EBSD analyses, the coating revealed no Kikuchi pattern and was deemed amorphous, while the substrate demonstrated an hcp Kikuchi pattern as for α-Ti.

3.2 | EPD as drug loading

Pipetting a drug solution over nanotubes and drying has been used for drug loading by others,[44] however, it is time and drug consuming.

Due to the positive charge of gentamicin and chitosan in solutions with pH below their pKa values, both can be deposited by applying a negative potential to the Ti wire. EPD performed with different voltages and time were compared for gentamicin deposition. Figure 2A shows that the amount of drug in the solution determined by UV spectroscopy corresponded to around 85%–90% of the weight increase measured after loading. The two values showed linear correlation, with $R^2 = 0.9952$ and equation:

$$\text{Drug (UV)} = 0.9968 * \text{Drug (Weight)} + 34.869. \quad (1)$$

With a slope of 0.9968 between the difference in weight and the drug amount measured by UV–vis, it can be concluded that the increase in weight was due to the drug loaded and not to some alteration of the oxide layer.

Next, the amount of drug loaded was correlated to the voltage applied and to the duration of the experiment to build a multiple linear regression model between the parameters of the loading procedure. The values considered in the analysis are shown in Figure 2C. The results were characterized by an $R^2 = 0.9335$, indicating that 93.35% of the variation in weight can be explained by the difference in voltage applied and by the time of the process. Significance $F = 0.001138$ indicated that the combination of voltage and time had statistically significant association with the difference in weight. The final equation given by the regression model is as follows:

$$\text{Weight [µg]} = 39.79 * \text{Voltage [V]} + 62.26 * \text{Time [min]} - 273.85. \quad (2)$$

As shown, almost 94% of the data are consistent with the model and both time ($p < .0001$) and voltage ($p = 0.0478$) can be considered significant factors in determining the final amount of drug loaded. Equation (2) can be used to calculate the required EPD parameters to obtain the desired amount of drug loaded into the nanotubes (µg), considering the voltage difference (V), and the time (min).

Overall, we observed that ADM resulted in a markedly lower gentamicin load compared to EPD with all parameters tested (deposition with ADM was an average of 83.63 µg (by weight) and 104.12 µg (by UV–vis)), therefore, EPD proved to be an efficient method for drug deposition.

SEM in combination with EDS was performed at selected pores (Figure 2 D, E). The spectra obtained corresponded to the components of the titanium alloy (Ti, Al, and V). In addition, Fluorine (F) was detected, as a remaining product from the anodization process. The presence of Sulfur (S) provided proof that gentamicin sulfate entered the nanotubes.

3.3 | Drug release

Recording the optical density of gentamicin solutions with known concentrations at 380 nm resulted in a standard curve (Figure 3A). The amount of drug in the release solution was calculated with the following equation derived from linear regression:

$$\text{Absorbance} = 0.000502 * \text{concentration} + 0.018683. \quad (3)$$

Fractional volume sampling was carried out for 3 days. Figure 3 B illustrates the gentamicin concentration in the release solution, Figure 3 C represents the cumulative release of gentamicin. We observed an initial burst release of around 78% in the first 10 min, then gentamicin was released at a slower rate for up to 3 days. The drug concentration stayed above the MIC determined in our system for the entire period tested and a cumulative amount of 400–550 µg gentamicin was detected. To characterize the mechanism of drug release, the release data were fitted to the Korsmeyer-Peppas equation:

$$Q = kt^n, \quad (4)$$

where Q stands for the percent drug release at time t, k is a release constant characterizing the device and n is a diffusional exponent. We found n to be 0.039 indicating a release mechanism driven primarily by Fickian diffusion.

We observed that the application of low molecular weight chitosan and TPP-crosslinking allowed for a continuous drug release for up

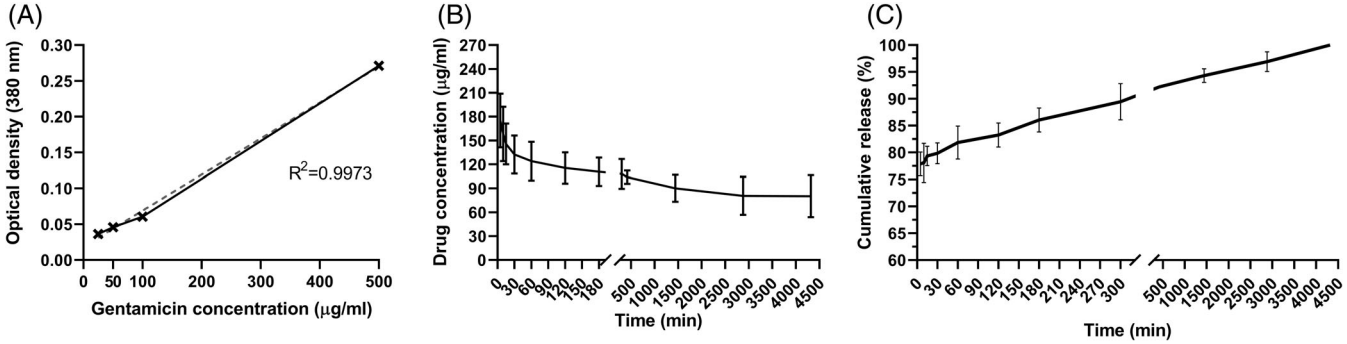

FIGURE 3 Gentamicin release from chitosan coated Ti nanotubes. (A) Gentamicin standard curve and linear regression (optical density at 380 nm), (B) Gentamicin concentration in the release medium (µg/ml), and (C) cumulative release of gentamicin (%).

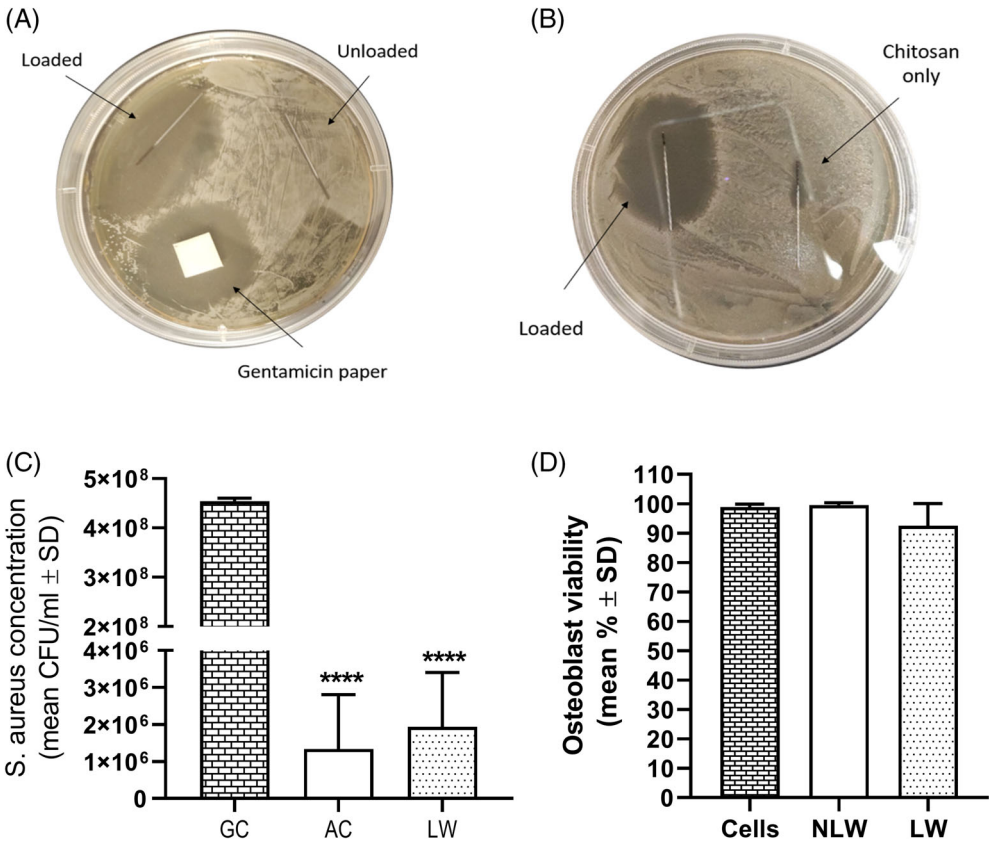

FIGURE 4 Antibacterial effect and cell compatibility of gentamicin-loaded nanotubes. (A–B) Agar diffusion assay comparing gentamicin-loaded, unloaded and chitosan-coated wires and a gentamicin soaked filter paper, (C) *S. aureus* growth in the presence of gentamicin-loaded nanotubes (GC, growth control; AC, antibiotic control; LW, loaded wire, $n = 3$, ****$p < .0001$ vs. GC, one-way ANOVA), and (D) Osteoblast viability after 24 h culture without wire (cells) or with non-loaded wire (NLW) and loaded wire (LW), Mean % ± SD, $p > .05$, one-way ANOVA, n = 3).

to 3 days. When wires coated with chitosan only were tested, we found consistently low absorbance values in the release medium, corresponding to not more than 10 µg gentamicin. Compared to the total released gentamicin amount (501.5 ± 0.707 µg), this interference would mean 2% difference and was disregarded in subsequent experiments.

3.4 | In vitro antibacterial effect of gentamicin loaded Ti wires

We found a gentamicin MIC of 3.6 µg/mL against *S. aureus* Xen36. In the agar diffusion assay, we observed an elliptical shaped IZ around the loaded wire (35 mm shorter and 45 mm longer axis) (Figure 4A). No IZ was observed around the unloaded wire, thus indicating that the presence of nanotubes alone did not inhibit bacterial growth. The gentamicin-soaked filter paper resulted in an IZ of 30 mm in diameter, confirming the effectivity of gentamicin sulfate to inhibit *S. aureus* growth. In a separate set, an EPD process with a solution containing chitosan only was performed to investigate if an only chitosan-coated wire has any antibacterial effect (Figure 4 B). It can be observed that the elliptical IZ around the drug-loaded wire was comparable to the previous one in Figure 4 A. A very small IZ was found around the chitosan-coated wire. This is in accordance with the natural antibacterial effect of chitosan described by others.[45]

In the liquid culture assay (Figure 4 C), we found that both AC and LW significantly decreased bacterial density compared to GC, further confirming the antibacterial effect of the loaded wire.

3.5 | Osteoblast viability

Figure 4 D illustrates the percent viable cells compared to the total number of mouse MC3T3-E1 cells after 24 h of incubation with anodized, non-loaded wire (NLW), gentamicin-loaded wire (LW) or without wire (Cells). While we observed a lower cell viability in the LW group, the difference was not statistically significant between the groups (cells 98.86%, NLW 99.5%, and LW 92.56%, respectively). Therefore, we believe that the gentamicin-loaded chitosan-coated Ti wires are effective against *S. aureus* without significantly affecting the viability of healthy cells. Future plans include the implantation of the device into the infected femur of mice to test its antibacterial behavior against *S. aureus* in our in vivo PJI model.[26]

4 | CONCLUSION

The current study has several strengths, including the creation of Ti nanotubes and EPD of gentamicin and chitosan. Our results indicate that TiO_2 nanotubes created on an implantable Ti wire are suitable for local drug delivery and prevention of PJI. Furthermore, two-step EPD

proved to be an effective and fast method for drug loading and coating and might represent a helpful tool for the development of local drug delivery systems. However, our study is not without limitations. Drug release was followed for 3 days, and future experiments are needed to evaluate the release over a longer time course. In addition, a limited evaluation of osteoblast viability was performed; additional experiments are necessary to exclude potential cytotoxicity over a longer period.

ACKNOWLEDGMENTS

The authors thank Dr. Mozart Q. Neto (microstructure of TiAlV), Dr. Jitesh Pratap, Marcus Winogradzki (donation and guidance on MC3T3-E1 cells), Dr. Sasha H. Shafikhani (guidance on *S. aureus* culture) and Sofia Gianotti.

FUNDING INFORMATION

The work was supported by the Grainger Directorship of the Rush Arthritis and Orthopedics Institute (PI: MAW). This research did not receive any specific grant from funding agencies in the public, commercial, or not-for-profit sectors.

DATA AVAILABILITY STATEMENT

The data that support the findings of this study are available from the corresponding author upon reasonable request.

ORCID

Adrienn Markovics https://orcid.org/0000-0003-4913-845X
Markus A. Wimmer https://orcid.org/0000-0001-6169-3873

REFERENCES

1. Fingar KR (Truven Health Analytics), Stocks C (AHRQ), Weiss AJ (Truven Health Analytics), Steiner CA (AHRQ). Most Frequent Operating Room Procedures Performed in U.S. Hospitals, 2003–2012. *Statistical Brief #186. Healthcare Cost and Utilization Project (HCUP) Statistical Briefs*; Agency for Healthcare Research and Quality, Rockville, MD. December 2014.
2. Postler A, Lutzner C, Beyer F, Tille E, Lutzner J. Analysis of Total knee arthroplasty revision causes. *BMC Musculoskelet Disord*. 2018;19(1):55. doi:10.1186/s12891-018-1977-y
3. Tan TL, Maltenfort MG, Chen AF, et al. Development and evaluation of a preoperative risk calculator for Periprosthetic joint infection following Total joint arthroplasty. *J Bone Joint Surg Am*. 2018;100(9):777-785. doi:10.2106/JBJS.16.01435
4. Montanaro L, Speziale P, Campoccia D, et al. Scenery of staphylococcus implant infections in orthopedics. *Future Microbiol*. 2011;6(11):1329-1349. doi:10.2217/fmb.11.117 PubMed PMID: 22082292.
5. Tande AJ, Patel R. Prosthetic joint infection. *Clin Microbiol Rev*. 2014;27(2):302-345. doi:10.1128/CMR.00111-13
6. Del Pozo JL, Patel R. Clinical practice. Infection associated with prosthetic joints. *N Engl J Med*. 2009;361(8):787-794. doi:10.1056/NEJMcp0905029
7. Izakovicova P, Borens O, Trampuz A. Periprosthetic joint infection: current concepts and outlook. *EFORT Open Rev*. 2019;4(7):482-494. doi:10.1302/2058-5241.4.180092
8. Allegranzi B, Zayed B, Bischoff P, et al. New WHO recommendations on intraoperative and postoperative measures for surgical site infection prevention: an evidence-based global perspective. *Lancet Infect Dis*. 2016;16(12):e288-e303. doi:10.1016/S1473-3099(16)30402-9
9. Moriarty TF, Kuehl R, Coenye T, et al. Orthopaedic device-related infection: current and future interventions for improved prevention and treatment. *EFORT Open Rev*. 2016;1(4):89-99. doi:10.1302/2058-5241.1.000037
10. Mainardes RM, Silva LP. Drug delivery systems: past, present, and future. *Curr Drug Targets*. 2004;5(5):449-455. doi:10.2174/1389450043345407
11. Kelly MP, Gililland JM, Blackburn BE, Anderson LA, Pelt CE, Certain LK. Extended Oral antibiotics increase bacterial resistance in patients who fail 2-stage exchange for Periprosthetic joint infection. *J Arthroplasty*. 2022;37:S989-S996. doi:10.1016/j.arth.2022.01.027. PubMed PMID: 35074446.
12. Leta TH, Gjertsen J, Dale H, et al. Antibiotic-loaded bone cement in prevention of Periprosthetic joint infections in primary Total knee arthroplasty: a register-based multicentre randomised controlled non-inferiority trial (ALBA trial). *BMJ Open*. 2021;11:e041096. doi:10.1136/bmjopen-2020-041096
13. Barth RE, Vogely HC, Hoepelman AI, Peters EJ. 'To bead or not to bead?' treatment of osteomyelitis and prosthetic joint-associated infections with gentamicin bead chains. *Int J Antimicrob Agents*. 2011;38(5):371-375. doi:10.1016/j.ijantimicag.2011.03.008
14. Geurts JA, Janssen DM, Kessels AG, Walenkamp GH. Good results in postoperative and hematogenous deep infections of 89 stable total hip and knee replacements with retention of prosthesis and local antibiotics. *Acta Orthop*. 2013;84(6):509-516. doi:10.3109/17453674.2013.858288
15. Pawlik A, Jarosz M, Syrek K, Sulka GD. Co-delivery of ibuprofen and gentamicin from nanoporous anodic titanium dioxide layers. *Colloids Surf B Biointerfaces*. 2017;152:95-102. doi:10.1016/j.colsurfb.2017.01.011
16. Kaur M, Singh K. Review on titanium and titanium based alloys as biomaterials for orthopaedic applications. *Mater Sci Eng C Mater Biol Appl*. 2019;102:844-862. doi:10.1016/j.msec.2019.04.064
17. Diebold U. Structure and properties of TiO_2 surfaces: a brief review. *Appl Phys A*. 2003;76:681-687.
18. Su EP, Justin DF, Pratt CR, et al. Effects of titanium nanotubes on the osseointegration, cell differentiation, mineralisation and antibacterial properties of orthopaedic implant surfaces. *Bone Joint J*. 2018;100B(1 Suppl. A):9-16. doi:10.1302/0301-620X.100B1.BJJ-2017-0551.R1
19. Debmalya G, Shahbazian-Yassar R, Shokuhfar T. Recent advances in nanotubes for orthopedic implants. *J Nanotech Smart Mater*. 2014;1(1).
20. Nie B, Long T, Ao H, Zhou J, Tang T, Yue B. Covalent immobilization of Enoxacin onto titanium implant surfaces for inhibiting multiple bacterial species infection and In vivo methicillin-resistant Staphylococcus aureus infection prophylaxis. *Antimicrob Agents Chemother*. 2016;61(1):e01766-16. doi:10.1128/AAC.01766-16
21. Zhang B, Braun BM, Skelly JD, Ayers DC, Song J. Significant suppression of Staphylococcus aureus colonization on intramedullary Ti6Al4V implants surface-grafted with vancomycin-bearing polymer brushes. *ACS Appl Mater Interfaces*. 2019;11(32):28641-28647. doi:10.1021/acsami.9b07648
22. Thompson K, Petkov S, Zeiter S, et al. Intraoperative loading of calcium phosphate-coated implants with gentamicin prevents experimental Staphylococcus aureus infection in vivo. *PloS One*. 2019;14(2):e0210402. doi:10.1371/journal.pone.0210402
23. Feng W, Geng Z, Li Z, et al. Controlled release behaviour and antibacterial effects of antibiotic-loaded titania nanotubes. *Mater Sci Eng C Mater Biol Appl*. 2016;62:105-112. doi:10.1016/j.msec.2016.01.046
24. Lin WT, Tan HL, Duan ZL, et al. Inhibited bacterial biofilm formation and improved osteogenic activity on gentamicin-loaded titania nanotubes with various diameters. *Int J Nanomedicine*. 2014;9:1215-30. doi:10.2147/IJN.S57875
25. Stavrakis AI, Niska JA, Loftin AH, Billi F, Bernthal NM. Understanding infection: a primer on animal models of periprosthetic joint infection. *Scient World J*. 2013;2013:1-6. doi:10.1155/2013/925906
26. Jie K, Deng P, Cao H, Feng W, Chen J, Zeng Y. Prosthesis design of animal models of periprosthetic joint infection following total knee

arthroplasty: a systematic review. *PloS One*. 2019;14(10):e0223402. doi:10.1371/journal.pone.0223402
27. Bernthal NM, Stavrakis AI, Billi F, et al. A mouse model of post-arthroplasty Staphylococcus aureus joint infection to evaluate in vivo the efficacy of antimicrobial implant coatings. *PLoS One*. 2010;5(9):e12580. doi:10.1371/journal.pone.0012580
28. Hamilton JL, Mohamed MF, Witt BR, Wimmer MA, Shafikhani SH. Therapeutic assessment of *N*-formyl-methionyl-leucyl-phenylalanine (fMLP) in reducing periprosthetic joint infection. *Eur Cell Mater*. 2021;42:122-138. doi:10.22203/eCM.v042a09
29. Cipriano AF, Miller C, Liu H. Anodic growth and biomedical applications of TiO2 nanotubes. *J Biomed Nanotechnol*. 2014;10(10):2977-3003. doi:10.1166/jbn.2014.1927
30. Roy P, Berger S, Schmuki P. TiO2 nanotubes: synthesis and applications. *Angew Chem*. 2011;50(13):2904-2939. doi:10.1002/anie.201001374
31. Sofia A, Alves ALR, Ribeiro AR, et al. A first insight on the biofunctionalization mechanisms of TiO_2 nanotubes with calcium, phosphorous and zinc by reverse polarization anodization. *Surf Coat Technol*. 2017;324:153-166.
32. Sofia A, Alves SBP, Sukotjo C, et al. Synthesis of calcium-phosphorous doped TiO2 nanotubes by anodization and reverse polarization: a promising strategy for an efficient biofunctional implant surface. *Appl Surf Sci*. 2017;399:682-701.
33. Cheung RC, Ng TB, Wong JH, Chan WY. Chitosan: an update on potential biomedical and pharmaceutical applications. *Mar Drugs*. 2015;13(8):5156-5186. doi:10.3390/md13085156
34. Martins AF, de Oliveira DM, Pereira AG, Rubira AF, Muniz EC. Chitosan/TPP microparticles obtained by microemulsion method applied in controlled release of heparin. *Int J Biol Macromol*. 2012;51(5):1127-1133. doi:10.1016/j.ijbiomac.2012.08.032
35. Ding P, Huang KL, Li GY, Liu YF. Preparation and properties of modified chitosan as potential matrix materials for drug sustained-release beads. *Int J Biol Macromol*. 2007;41(2):125-131. doi:10.1016/j.ijbiomac.2006.12.008
36. Pal D, Nayak AK, Saha S. Interpenetrating polymer network hydrogels of chitosan: applications in controlling drug release. In: Guo S, ed. *Cellulose-Based Superabsorbent Hydrogels Polymers and Polymeric Composites: A Reference Series*. Springer; 2018.
37. Gupta K, Jabrail, F. Controlled-release formulations for hydroxy urea and rifampicin using polyphosphate-anion-crosslinked chitosan microspheres. *J Appl Polym Sci*. 2007;104:1942-1956. doi:10.1002/app.25881
38. Zhu Y, Marin LM, Xiao Y, Gillies ER, Siqueira WL. pH-sensitive chitosan nanoparticles for salivary protein delivery. *Nanomaterials (Basel)*. 2021;11(4):1028. doi:10.3390/nano11041028
39. Frutos P, Torrado S, Perez-Lorenzo ME, Frutos G. A validated quantitative colorimetric assay for gentamicin. *J Pharm Biomed Anal*. 2000;21(6):1149-1159. doi:10.1016/s0731-7085(99)00192-2
40. Wiegand I, Hilpert K, Hancock RE. Agar and broth dilution methods to determine the minimal inhibitory concentration (MIC) of antimicrobial substances. *Nat Protoc*. 2008;3(2):163-175. doi:10.1038/nprot.2007.521
41. Heatley NG. A method for the assay of penicillin. *Biochem J*. 1944;38(1):61-65. doi:10.1042/bj0380061
42. Regonini DBC, Jaroenworaluck A, Stevens R. 'A review of growth mechanism, structure and crystallinity of anodized TiO2 nanotubes. *Mater Sci Eng*. 2013;74(12):377-406. doi:10.1016/j.mser.2013.10.001
43. Karan Gulati AS, Findlay D, Losic D. Optimizing anodization conditions for the growth of Titania nanotubes on curved surfaces. *J Phys Chem C*. 2015;119(28):16033-16045.
44. Çalışkan N, Bayram C, Erdal E, Karahaliloğlu Z, Denkbaş EB. Titania nanotubes with adjustable dimensions for drug reservoir sites and enhanced cell adhesion. *Mater Sci Eng C*. 2014;35:100-105. doi:10.1016/j.msec.2013.10.033
45. Shen J, Jin B, Qi YC, Jiang QY, Gao XF. Carboxylated chitosan/silver-hydroxyapatite hybrid microspheres with improved antibacterial activity and cytocompatibility. *Mater Sci Eng C Mater Biol Appl*. 2017;78:589-597. doi:10.1016/j.msec.2017.03.100

SUPPORTING INFORMATION

Additional supporting information can be found online in the Supporting Information section at the end of this article.

How to cite this article: Della Fara G, Markovics A, Radice S, et al. Electrophoretic deposition of gentamicin and chitosan into titanium nanotubes to target periprosthetic joint infection. *J Biomed Mater Res*. 2023;111(9):1697-1704. doi:10.1002/jbm.b.35267